Letters on Materials 15 (4), 2025 pp. 304-310 www.lettersonmaterials.com

Received 31 August 2025; Accepted 23 October 2025
https://doi.org/10.48612/letters/2025-4-304-310 https://elibrary.ru/tiwkfo

Effect of thermal aging on strengthening mechanisms of 12% Cr ferritic-martensitic steel

N. A. Polekhina†, V. V. Osipova, S. A. Akkuzin, I. Yu. Litovchenko

†nap@ispms.ru

Institute of Strength Physics and Materials Science of the Siberian Branch of the Russian Academy of Sciences, Tomsk 634055, Russia

Abstract: A systematic investigation of the evolution of microstructure, mechanical properties, and strengthening mechanisms of 12% chromium ferritic-martensitic steel 16Cr12MnWSiVNbB (EP-823-Sh type) during long-term thermal aging (up to 5000 hrs) at temperatures of 450 – 580°C was conducted. Comprehensive electron microscopy analysis revealed quantitative changes in the structural parameters of the steel after aging compared to the initial state: a 30% increase in ferrite grain size, a 1.3 – 1.7-fold reduction in dislocation density, coagulation of $M_{23}C_6$ carbides, and depletion of Mo in the solid solution. Qualitative changes include heterogeneous precipitation of Laves phase $(Fe,Cr)_2(Mo,W)$ particles after aging at 580°C for 5000 hrs. A quantitative assessment was performed to determine the contributions of individual strengthening mechanisms to the yield strength of the steel under various aging conditions. It was established that the reduction in strength properties after aging is due to weakening of dislocation and grain boundary strengthening mechanisms. The increase in yield strength after prolonged (5000 hrs) aging at 580°C is attributed to the compensatory effect of precipitation strengthening resulting from the formation of finely dispersed Laves phase particles. The obtained results are of significant importance for predicting the long-term operational durability of ferritic-martensitic steels in power engineering applications.

Keywords: ferritic-martensitic steel, thermal stability, microstructure, mechanical properties, long-term aging, strengthening mechanisms

Acknowledgements: *This study was funded by the Russian Science Foundation; Project No. 24-29-00431, https://rscf.ru/project/24-29-00431/.*

1. Introduction

Ferritic-martensitic steels containing 9 – 12% Cr represent key structural materials for advanced power generation systems owing to their optimal combination of irradiation and corrosion resistance, mechanical strength, and thermal stability [1 – 7]. The Russian steel grade 16Cr12MnWSiVNbB (EP-823-Sh) is especially promising for use in reactor core components designed for long-term service at temperatures reaching 620°C [5 – 12].

During prolonged high-temperature exposure, the microstructure of these steels undergoes substantial evolution, characterized by dislocation structure relaxation, coarsening of strengthening phases, precipitation of intermetallic phases, and redistribution of alloying elements [7,12,13 – 23]. These microstructural changes govern the evolution of key strengthening mechanisms, thereby determining the mechanical performance of the steel under long-term service conditions [1,13 – 23].

Despite extensive research on the thermal stability of high-chromium ferritic-martensitic steels [7,12,15 – 24], a systematic analysis of the coupled effects of aging temperature and duration on the evolution of individual strengthening mechanisms including solid solution, precipitation, dislocation, and grain boundary strengthening, remains insufficiently explored in the scientific literature.

This work presents a comprehensive investigation of the effects of aging parameters (450 – 580°C, 1000 – 5000 hrs) on the microstructure and mechanical properties of 12% Cr ferritic-martensitic steel 16Cr12MnWSiVNbB, with a particular emphasis on quantitative evaluation of the contributions of individual strengthening mechanisms to the overall strength.

2. Materials and experimental method

The elemental composition of the steel under study is presented in Table 1. Aging was carried out on flat samples at 450°C for 5000 hrs (AG450/5000), at 540°C for 1000 hrs (AG540/1000), at 580°C for 1000 and 5000 hrs (AG580/1000 and AG580/5000) in sealed glass tubes in Ar environment. Initial samples were sheets with a thickness of 2 mm in the as-received (AR) state.

Table 1. Elemental composition of steel (wt.%, base Fe).

C	Cr	Mn	Mo	Nb	V	W	Ni	N	Si	Ce	Ti	B	Al
0.14	11.56	0.58	0.74	0.40	0.34	0.68	0.68	0.03	1.09	0.10	0.01	0.006	0.02

The grain-subgrain microstructure and second phase particles of the steel were studied by scanning electron microscopy (SEM), including the electron backscatter diffraction method (EBSD), an Apreo 2 S SEM equipped with a Field Emission Gun and a Pegasus Integrated EDX-EBSD system with the Octane Elect Super and Velocity Super detectors (EDAX). The samples for SEM investigations were etched in a Vilella's reagent (5 ml HCl, 1 g picric acid, 100 ml ethanol).

Prior austenite grain (PAG) sizes were measured from SEM images using the linear intercept method. The size distribution, number density, and volume fraction of second-phase particles were quantified from SEM backscattered electron (BSE) images using ImageJ software.

The transmission electron microscopy (TEM) studies were carried out using thin foils and carbon replicas on a JEOL JEM-2100 microscope (accelerating voltage 200 kV) equipped with an X-ray energy dispersive microanalysis system (EDX, INCA Energy). Thin foils were prepared by electrolytic polishing in a 10% solution of chromic anhydride (CrO_3) in phosphoric acid (H_3PO_4).

The mechanical tensile tests were carried out at a strain rate of $\approx 2\times10^{-3}$ s^{-1} on a MIM 2-50 testing machine at 20°C. We used dogbone-shaped samples with a gage section of $13.0\times2.0\times1.0$ mm.

3. Results

Microstructural evolution of ferritic-martensitic steel 16Cr12MnWSiVNbB following aging treatments at 450 and 540°C was initially investigated in prior studies [7,12].

Comparative SEM and TEM studies of the microstructure of the steel in the as-received condition and after aging at 450–580°C (for 1000–5000 hrs) revealed a hierarchically organized structure dispersion-strengthened by second-phase particles in all structural states (Figs. 1–4). Within prior austenite grains measuring 13.5–14.7 μm (Fig. 1, Table 2), there are ferrite grains and subgrains with a high dislocation density (up to $\rho \approx 6.1\times10^{14}$ m^{-2}, Fig. 4). The carbide subsystem in the initial state consists of rounded MX-type particles (M — Nb, Mo, V, etc.; X — C, N) located inside grains and subgrains, and predominantly submicron-sized Cr-rich $M_{23}C_6$ carbides (M — Cr, Fe, Mo, W, etc.) with irregular morphology located predominantly along the boundaries of structural elements (Figs. 2–4, Table 2).

Aging at 450°C (5000 hrs), 540°C (1000 hrs), and 580°C (1000 hrs) resulted only in quantitative changes in structural parameters of the steel (Table 2, Figs. 1–4). In contrast, prolonged exposure at 580°C additionally induced qualitative transformations in its phase composition (Figs. 2, 4). The key microstructural changes observed after aging, compared to the initial state, are as follows (Table 2, Figs. 1–4):

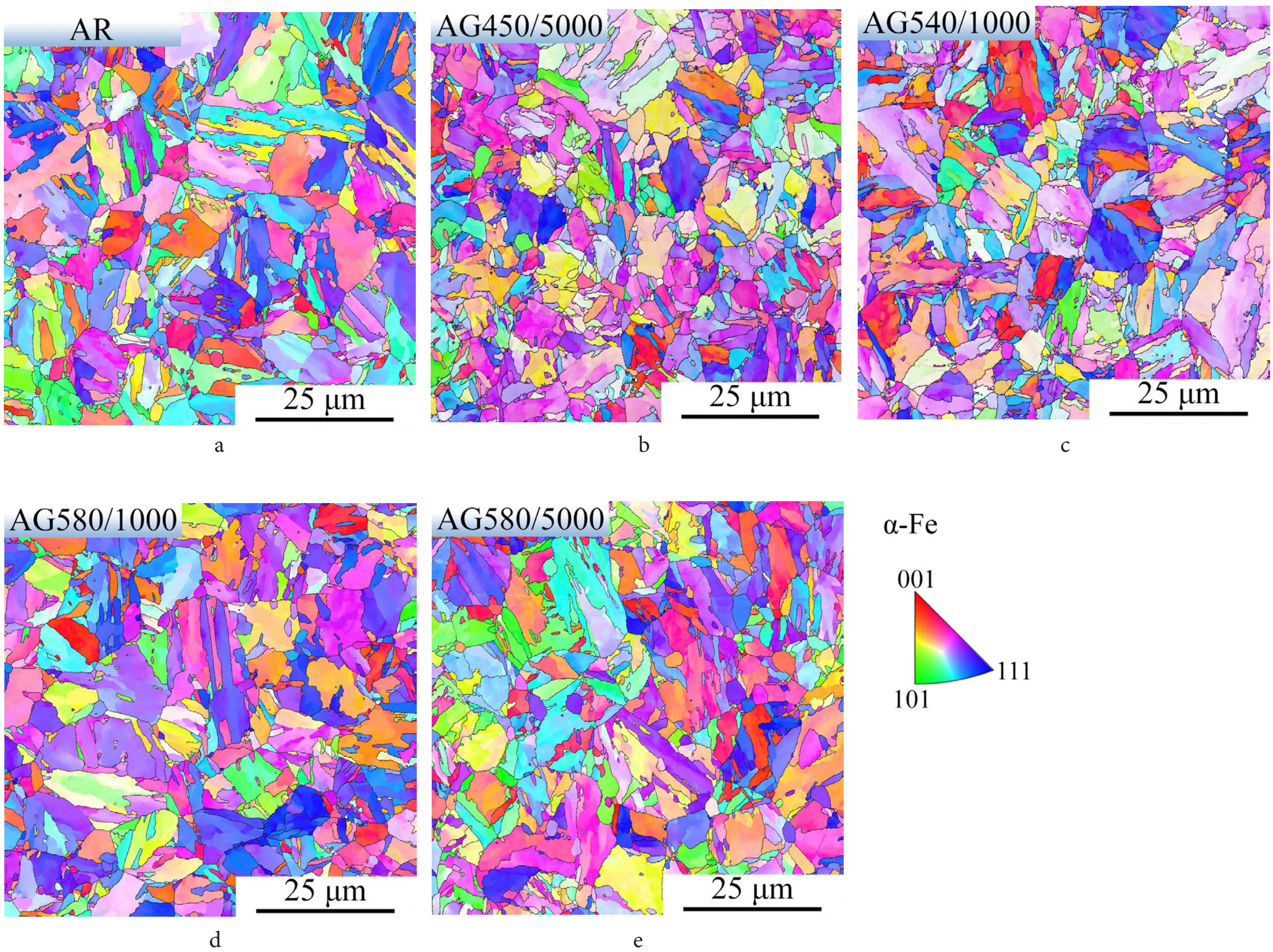

Fig. 1. (Color online) Inverse pole figure (IPF) EBSD images of steel microstructure in AR state (a) and after aging at 450°C for 5000 hrs (b), at 540°C for 1000 hrs (c), at 580°C for 1000 and 5000 hrs (d and e, respectively).

Table 2. Microstructure parameters of as-received steel and after aging at different temperatures.

Structural state	AR	AG450/5000	AG540/1000	AG580/1000	AG580/5000
Average size of PAGs, μm	14.7 ± 0.7	14.8 ± 0.7	13.5 ± 0.5	14.3 ± 0.8	14.7 ± 0.5
Average size of ferrite grains, μm	1.33 ± 0.1	1.68 ± 0.1	1.78 ± 0.1	1.72 ± 0.1	1.74 ± 0.1
Dislocation density, $\times 10^{14}$ m^{-2}	6.1 ± 0.1	4.7 ± 0.1	3.5 ± 0.1	4.1 ± 0.1	3.8 ± 0.1
Average size of $M_{23}C_6$, nm	217 ± 13	257 ± 15	261 ± 15	235 ± 11	219 ± 10*
Volume fraction of $M_{23}C_6$, %	1.6 ± 0.1	2.7 ± 0.2	2.8 ± 0.2	2.65 ± 0.2	2.75 ± 0.1*
Number density of $M_{23}C_6$, μm^{-2}	1.40 ± 0.08	1.34 ± 0.10	1.23 ± 0.07	1.65 ± 0.32	2.43 ± 0.44*
Average size of MX, nm	252 ± 17	248 ± 15	254 ± 16	254 ± 13	255 ± 11
Volume fraction of MX, %	0.3 ± 0.1	0.3 ± 0.1	0.3 ± 0.1	0.3 ± 0.1	0.3 ± 0.1
Mo content in matrix according to EDX data, at.%	0.64 ± 0.05	0.35 ± 0.03	0.41 ± 0.06	0.29 ± 0.05	0.23 ± 0.04

*total values for $M_{23}C_6$ carbides and Laves phase particles are given.

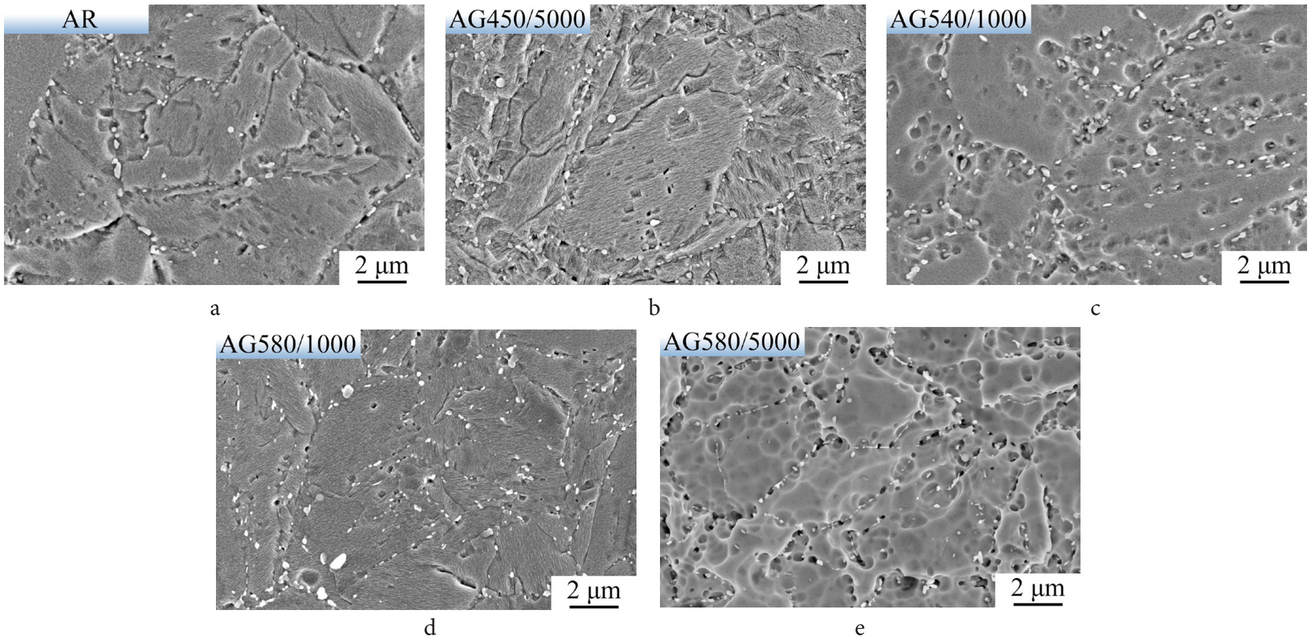

Fig. 2. SEM images of steel microstructure with second phase particles in AR state (a) and after aging at 450°C for 5000 hrs (b), at 540°C for 1000 hrs (c), at 580°C for 1000 and 5000 hrs (d and e, respectively).

– an approximately 1.3-fold increase in the ferrite grain size;

– an approximately 1.3–1.7-fold reduction in the dislocation density due to recovery and polygonization processes;

– an increase in the size (by less than 44 nm) and volume fraction (by less than 1.8-fold) of $M_{23}C_6$ particles, accompanied by a change in their number density due to additional precipitation and coarsening via the Ostwald ripening mechanism.;

– an increase in the Mo content of the $M_{23}C_6$ particles (from 4.5 – 8.3 to 10.1–16.2 wt.%) and a corresponding depletion of this element in the matrix solid solution;

– precipitation of Mo-rich Laves phase $(Fe, Cr)_2(Mo, W)$, following a 5000 hrs incubation period at 580°C. These particles, which were absent in other investigated structural states, nucleate heterogeneously at prior austenite grain boundaries, ferrite grain and subgrain boundaries (often adopting a lens shape morphology), and on existing $M_{23}C_6$ particles, forming irregular shell-like structures around them. The formation of these intermetallic phase particles further contributes to the depletion of Mo from the solid solution.

Of a particular interest is the exceptional thermal stability of MX-type particles, which maintain nearly constant size and volume fraction even after prolonged aging at 450 – 580°C for up to 5000 hrs (Table 2).

Figure 3 presents histograms showing the size distribution of secondary phase particles. Notably, after aging at 580°C for 5000 hrs, the distribution includes both $M_{23}C_6$ carbides and Laves phase particles due to the difficulty in experimentally distinguishing them in SEM images. As evident from the Fig. 3, aging under these conditions increases the fraction of particles smaller than 100 nm compared to the initial state and other aging regimes, which is attributed to the precipitation of finely dispersed Laves phase particles.

Analysis of short-term tensile test data presented in Table 3 demonstrates that thermal aging of the steel in the 450 – 580°C range reduces its yield strength by up to 127 MPa. This decrease exhibits a complex non-linear dependence on both aging temperature and duration. To establish a correlation between the microstructural evolution and mechanical properties, a quantitative assessment of the contributions from key strengthening mechanisms was performed, based on the experimentally determined structural parameters provided in Table 2.

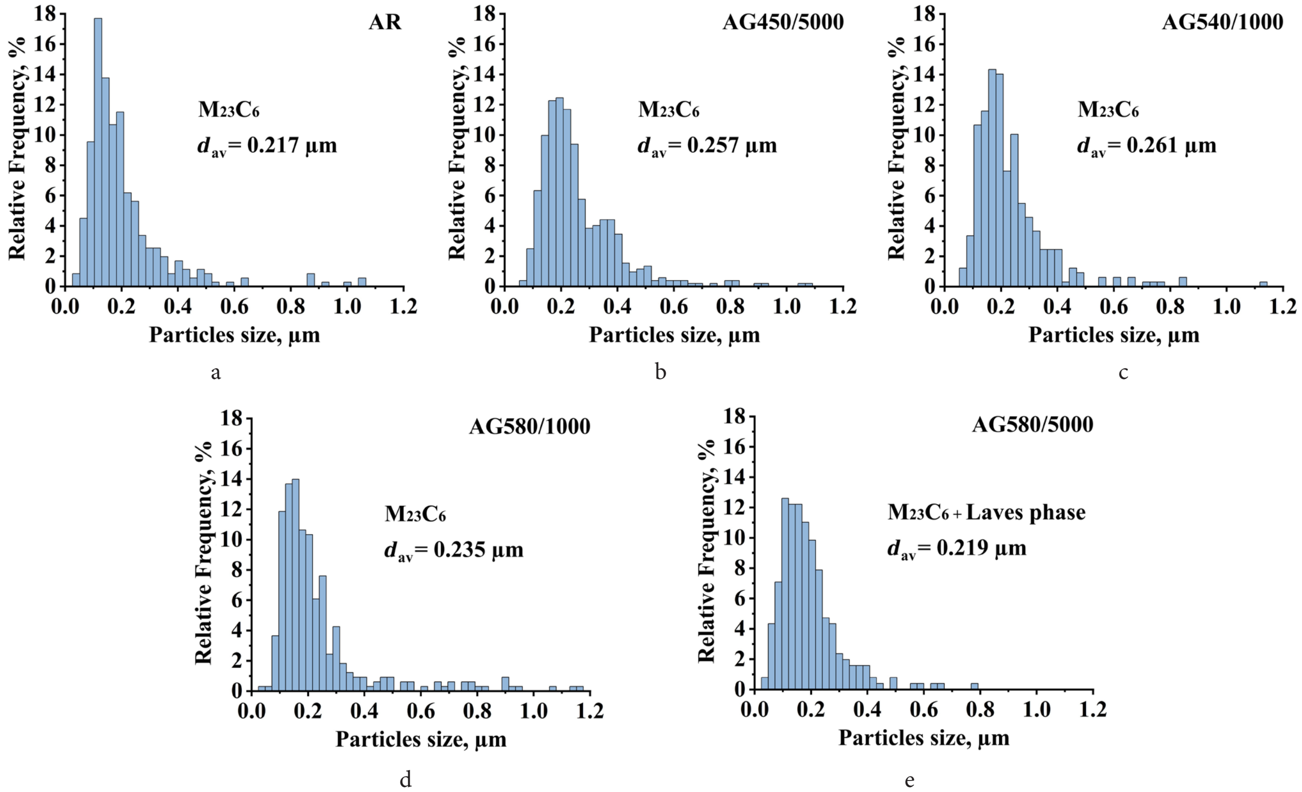

Fig. 3. Size distribution of secondary phase particles in the steel in the as-received (AR) condition and after aging at 450–580°C for 1000–5000 hrs.

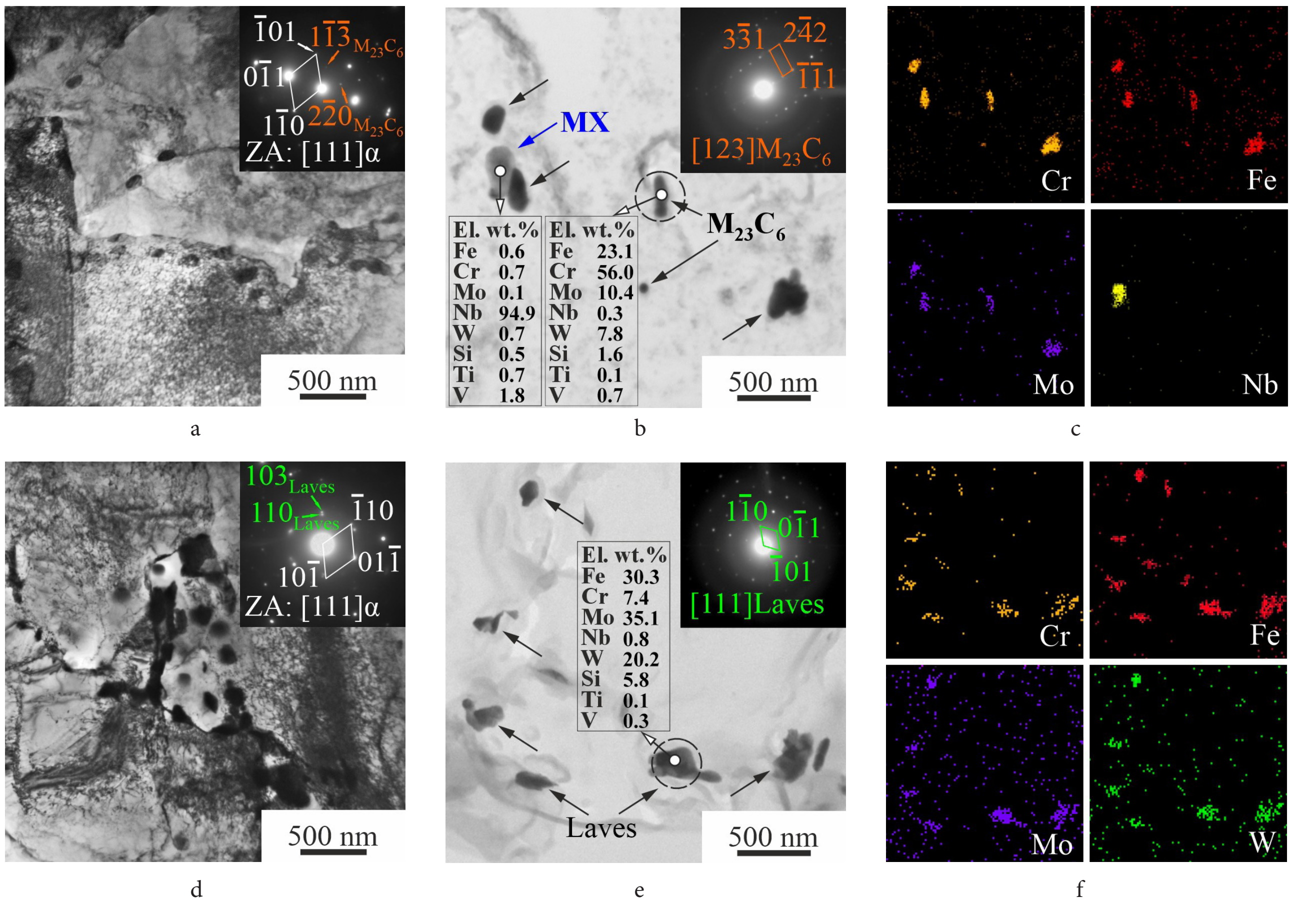

Fig. 4. (Color online) TEM images of the steel microstructure after aging at 540°C for 1000 hrs and 580°C for 5000 hrs: bright-field images of grain-subgrain structure (a, d); bright-field images of secondary phase particles on a carbon replica (b, e); EDS element distribution maps corresponding to Fig. 3b, e, respectively (c, f).

Table 3. Experimental yield strength ($\sigma_{0.2}^{exp}$) and estimated contributions of individual strengthening mechanisms to the calculated yield strength ($\sigma_{0.2}^{calc}$) of the steel in the as-received state and after aging at various temperatures.

State	AR	AG450/5000	AG540/1000	AG580/1000	AG580/5000
$\sigma_{0.2}^{exp}$, MPa	637	580	510	550	579
σ_0, MPa	30	30	30	30	30
σ_{ss}, MPa	130	112	115	108	104
σ_{gb}, MPa	266	237	230	234	233
σ_d, MPa	200	176	152	164	158
σ_{Or}, MPa	57	71	51	64	100
$\sigma_{0.2}^{calc}$	683	626	578	600	625

The yield strength of steels ($\sigma_{0.2}^{calc}$) can be represented as a linear superposition of key strengthening contributions: the intrinsic lattice friction stress (σ_0), solid solution strengthening (σ_{ss}), grain-boundary strengthening (σ_{gb}), dislocation strengthening (σ_{disl}) and precipitation strengthening (σ_{Or}). This relationship is expressed as follows [11, 23, 25]:

$$\sigma_{0.2}^{calc} = \sigma_0 + \sigma_{ss} + \sigma_{gb} + \sigma_{disl} + \sigma_{Or}. \quad (1)$$

The intrinsic lattice friction stress (σ_0), which originates from the Peierls-Nabarro barrier, is typically estimated using the established relationship [26]:

$$\sigma_0 = 2G \times 10^{-4}, \quad (2)$$

where G is the shear modulus (GPa). Using the value of $G = 85.3$ GPa [9] for the steel under investigation, the calculated contribution of σ_0 is approximately 30 MPa (Table 3 and Fig. 5). As a fundamental property of the crystal lattice, this value remains constant and is independent of the subsequent structural state of steel.

The solid solution strengthening from substitutional elements (σ_{ss}) in the bcc matrix was estimated for Cr, W, and Mo according to [18, 23, 28]:

$$\sigma_{ss} = 0.00689kX^n, \quad (3)$$

where X is the equilibrium concentration of substitutional elements (at.%), n is an exponent with a value of 0.75 for the elements considered, the constant 0.00689 is serves to convert the result from psi (pound per square inch) to MPa and k is the strengthening coefficient. The calculation rests on the assumption that nearly all C and Nb atoms are partitioned into carbide phases, thereby excluding them from the solid solution. The influence of all other alloying elements was neglected due to their low concentrations and/or the corresponding strengthening coefficient. The respective strengthening coefficients (k) for Cr, W, and Mo are 1400, 11000, and 9600 [28, 29]. The Mo concentration (X) is highly dependent on the aging mode, as evidenced by EDX data (Table 2). Aging at 450°C for 5000 hrs, at 540°C for 1000 hrs and at 580°C for 1000 hrs leads to Mo enrichment of $M_{23}C_6$ carbides. Aging at 580°C for 5000 hrs further depletes the matrix of Mo through the additional precipitation of Laves phase $(Fe, Cr)_2(Mo, W)$ particles. This progressive loss of Mo from the solid solution with aging time and temperature directly results in a corresponding decrease in the calculated σ_{ss} values, as presented in Table 3 and Fig. 5.

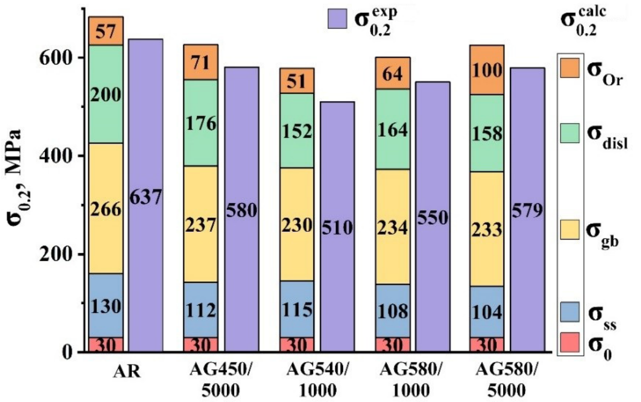

Fig. 5. (Color online) Comparison of the yield strength calculated by the linear summation of individual strengthening mechanisms ($\sigma_{0.2}^{calc}$) with experimentally measured values ($\sigma_{0.2}^{exp}$) for the steel in the as-received (AR) condition and after various aging treatments.

The grain boundary strengthening (σ_{gb}) can be expressed as following equation according to Hall-Petch relation [23, 25, 28]:

$$\sigma_{gb} = \frac{k_{gb}}{\sqrt{D}}, \quad (4)$$

where k_{gb} is a microstructural parameter (0.307 MPa × $m^{1/2}$) and D is the mean grain size. Analysis of EBSD data revealed that after aging the mean ferrite grain size increased by approximately 30% compared to the as-received condition (Table 2). This grain coarsening directly resulted in a corresponding decrease in the calculated σ_{gb} value, as detailed in Table 3 and Fig. 5.

The dislocation strengthening σ_{disl} can be described using Taylor theory as [24–26, 28]:

$$\sigma_{disl} = \alpha G b \sqrt{\rho}, \quad (5)$$

where α is a material-specific constant (taken as 0.38 for α-Fe [26]), G is the shear modulus, b is the Burgers vector magnitude (about 0.25 nm), and ρ is the total dislocation density (m^{-2}). The experimental results demonstrate that aging reduces the dislocation density (Table 2), leading to a decrease in the calculated dislocation strengthening contribution. This effect is accelerated at higher temperatures due to enhanced recovery and polygonization, as quantitatively shown by the results in Table 3 and Fig. 5.

According to Ashby-Orowan, precipitation strengthening of steel can be expressed as [25, 29]:

$$\sigma_{Or} = \frac{0.538Gb\sqrt{f}}{d} \times \ln\frac{d}{2b}, \quad (6)$$

where d is the average diameter of the precipitates and f is their volume fraction. The precipitation strengthening contribution was calculated based on the combined effect of all precipitate types present in each specific microstructural state. While thermally stable MX particles undergo minimal change after aging, the strengthening is primarily governed by the evolution of $M_{23}C_6$ carbides, which coarsen and increase in volume fraction (Table 2). An additional contribution arises from the precipitation of fine Laves phase particles after a prolonged incubation period (5000 hrs) at 580°C (Table 2). For example, particles with a size of 80 nm with a volume fraction of only ≈0.5% can provide an increase in the yield strength of steel by ≈50 MPa. The calculated σ_{Or} values for each structural state, which reflect this complex precipitate evolution, are presented in Table 3 and Fig. 5.

4. Discussion

As evidenced by the results of this study, the applied linear superposition model of individual strengthening contributions (Eq. (1)) enables highly accurate prediction of the yield strength of the investigated steel in both the as-received state and after various aging treatments. This is confirmed by the good agreement between the calculated ($\sigma_{0.2}^{calc}$) and experimentally determined ($\sigma_{0.2}^{exp}$) yield strength values (Table 3, Fig. 5).

The analysis reveals that the change in the yield strength of steel after aging is governed not by a single mechanism, but rather results from the complex interaction of several competing softening and strengthening processes activated by thermal exposure.

Following aging at 450°C for 5000 hrs, 540°C for 1000 hrs, and 580°C for 1000 hrs, softening processes dominate: the decrease in experimental yield strength is associated with a reduction in two primary strengthening mechanisms — dislocation (σ_{disl}) and grain boundary (σ_{gb}) strengthening (Table 3, Fig. 5). This is a direct consequence of the activation of recovery and polygonization processes, leading to the annihilation and redistribution of dislocations, as well as minor ferrite grain growth.

Concurrently, a decrease in the solid solution strengthening contribution (σ_{ss}) is observed (Table 3, Fig. 5), which is predominantly controlled by the concentration of Mo in the steel matrix. The gradual reduction in σ_{ss} with increasing aging temperature and time is a direct result of the progressive depletion of Mo from the solid solution. This depletion occurs through its redistribution into growing $M_{23}C_6$ carbides and Laves phase $(Fe, Cr)_2(Mo, W)$ particles that precipitate after aging at 580°C for 5000 hrs.

The reduction in σ_{disl}, σ_{gb}, and σ_{ss} is partially compensated by an increase in precipitation strengthening contribution (σ_{Or}) for most aged conditions, which is mainly attributed to the formation of new precipitates and an increased volume fraction of $M_{23}C_6$ carbides. The most significant increase in σ_{Or} is observed after prolonged aging at 580°C for 5000 hrs (Table 3, Fig. 5). This is explained by the formation of a high density of fine Laves phase particles and represents the key factor responsible for the anomalous growth of yield strength in this structural condition.

Thus, the presented analysis establishes a clear quantitative relationship between the evolution of microstructure and the mechanical properties of the steel. This work highlights the critical importance of accounting for the simultaneous evolution of all strengthening components for accurate prediction of the mechanical properties of advanced steels under long-term service conditions. The obtained results suggest that targeted microstructural control, particularly the formation of stable, finely dispersed precipitates that pin the dislocation substructure and/or prevent the migration of the boundaries of structural elements, can effectively counteract the softening mechanisms to maintain high strength after thermal exposure.

4. Conclusions

Long-term thermal aging (up to 5000 hrs) of the ferritic-martensitic steel 16Cr12MnWSiVNbB in the range of 450 – 580°C induces complex microstructural evolution. This transformation is characterized by the dislocation structure relaxation, ferrite grain growth, coagulation of $M_{23}C_6$ carbides, and redistribution of alloying elements between the matrix and second-phase particles, resulting in a decrease in the Mo content in the solid solution. A qualitative change in the phase composition involves the precipitation of Laves phase $(Fe, Cr)_2(Mo, W)$ intermetallic particles at 580°C after a prolonged incubation period (5000 hrs).

The regularities of change in the strength properties of the steel during thermal aging are determined by the competition of the ongoing processes of evolution in its structural-phase state. Estimates of the contributions of various strengthening mechanisms, based on experimentally determined structural parameters of the steel as a function of aging temperature and duration, showed that the decrease in its yield strength (by up to 127 MPa) compared to the initial state is primarily due to a reduction in the contributions of dislocation and grain boundary strengthening mechanisms. Precipitation strengthening associated with the formation of fine Laves phase particles has a compensatory effect, leading to an improvement in the strength properties of the studied steel after aging at 580°C for 5000 hrs.

The obtained results establish a correlation between thermal aging conditions and the evolution of microstructure and mechanical properties. This understanding provides a foundation for the targeted design of microstructure in heat-resistant steels to extend their high-temperature service life.

References

1. W. Yan, W. Wang, Y. Shan, K. Yang, W. Sha, 9-12Cr Heat-Resistant Steels, Springer International Publishing, 2015, 218 p.
2. R.G. Odette, S.J. Zinkle, Structural Alloys for Nuclear Energy Applications, Elsevier, 2019, 655 p.
3. F. Abe, Precipitate design for creep strengthening of 9% Cr tempered martensitic steel for ultra-supercritical power plants, Sci. Technol. Adv. Mater. 9 (2008) 013002.
4. C. Cabet, F. Dalle, E. Gaganidze, J. Henry, H. Tanigawa, Ferritic-martensitic steels for fission and fusion applications, J. Nucl. Mater. 523 (2019) 510 – 537.

5. I.Yu. Litovchenko, K.V. Almaeva, N.A. Polekhina, S.A. Akkuzin, V.V. Linnik, E.N. Moskvichev, V.M. Chernov, M.V. Leontyeva-Smirnova, The Microstructure and Mechanical Properties of Ferritic-Martensitic Steel EP-823 after High-Temperature Thermomechanical Treatment, Metals 12 (2022) 79.
6. N.A. Polekhina, I.Y. Litovchenko, K.V. Almaeva, S.A. Akkuzin, E.N. Moskvichev, V.M. Chernov, I.A. Naumenko, M.S. Saifutdinova, M.V. Leontieva-Smirnova, Special features of the surface layer structure of ferritic-martensitic EP-823-Sh steel after prolonged exposure to the flowing lead at 630°C under low oxygen concentration, J. Nucl. Mater. 572 (2022) 154039.
7. N. Polekhina, V. Osipova, K. Spiridonova, I. Litovchenko, S. Akkuzin, E. Moskvichev, V. Chernov, M. Leontyeva-Smirnova, Thermal stability of microstructure and mechanical properties of high chromium ferritic-martensitic steel at 450 and 540°C, Mater. Charact. 224 (2025) 115004.
8. V.F. Terent'ev, V.M. Chernov, A.G. Kolmakov, D.V. Prosvirnin, G.V. Kopiev, M.V. Leont'eva-Smirnova, K.A. Moroz, O.S. Antonova, Fatigue Strength of Ferrite-Martensite 12% Chromium Steels EK-181, EP-823 and Vanadium Alloy V-4Ti-4Cr, Inorg. Mater.: Appl. Res. 9 (2018) 212–220.
9. G.A. Birzhevoy, M.I. Zakharova, V.P. Tarasikov, The study of the formation of complexes of implementation and substitution atoms in EP-823 ferritic-martensitic steel at different heat treatment, Problems of nuclear science and technology. Series: materials science and new materials 2 (2019) 4–11. (in Russian)
10. M.Yu. Belomytsev, V.G. Molyarov, Investigation of Creep resistance of ferritic-martensitic steel 16Cr12MoWSiVNbB (EP-823), Izvestiya. Ferrous Metallurgy 62 (2019) 290–302. (in Russian)
11. K.V. Almaeva, I.Yu. Litovchenko, N.A. Polekhina, V.V. Linnik, Hardening Mechanisms of 12% Chromium Ferritic-Martensitic Steel EP-823, Steel in Translation 52 (12) (2022) 1135–1141.
12. N.A. Polekhina, V.V. Osipova, K.V. Spiridonova, I.Yu. Litovchenko, V.M. Chernov, M.V. Leontieva-Smirnova, N.S. Nikolaeva, Microstructure and mechanical properties of 12% Cr ferritic-martensitic steel after aging at 450°C during 5000 hours, Lett. Mater. 14 (4) (2024) 299–305.
13. K.C. Sahoo, J. Vanaja, P. Parameswaran, V.D. Vijayanand, K. Laha, Effect of Thermal Ageing on Microstructure, Tensile and Impact Properties of Reduced Activated Ferritic-Martensitic Steel, Mater. Sci. Eng. A 686 (2017) 54–64.
14. H. Ghassemi-Armaki, R.P. Chen, K. Maruyama, M. Yoshizawa, M. Igarashi, Static recovery of tempered lath martensite microstructures during long-term aging in 9–12% Cr heat resistant steels, Mater. Lett. 63 (2009) 2423–2425.
15. D.J. Sprouster, B. Adam, A. Koziol, L. Rolly, C. Huotilainen, J.D. Tucker, Long-term thermal aging effects in ferritic-martensitic steel HT9, Mater. Charact. 217 (2024) 114418.
16. X. Xiao, G. Liu, B. Hu, J. Wang, W. Ma, Microstructure Stability of V and Ta Microalloyed 12%Cr Reduced Activation Ferrite/Martensite Steel during Long-term Aging at 650°, J. Mater. Sci. Technol. 31 (2015) 311–319.
17. H. Kang, J. Shen, H. Han, S. Zhang, F. Hu, B. He, Q. Zhao, G. Xiao, Influence of long-term thermal ageing (>10,000 h) on low stress creep deformation of P92 heat-resistant steels, Mater. High Temp. 37 (2020) 196–206.
18. S. Ge, B. Niu, Z. Wang, Q. Pan, C. Liu, Q. Wang, Microstructural Stability and Mechanical Property of a Medium-Si 12% Cr Reduced Activation Ferritic/Martensitic Steel at High Temperatures, J. Mater. Eng. Perform. 31 (7) (2022) 5697–5705.
19. Yu. Xu, W. Li, M. Wang, X. Zhang, Y. Wu, N. Min, W. Liu, X. Jin, Nano-sized MX carbonitrides contribute to the stability of mechanical properties of martensite ferritic steel in the later stages of long-term aging, Acta Mater. 175 (2019) 148–159.
20. T. Yu, C. Liu, D. Wu, S. Wei, S. Lu, Microstructure and mechanical properties evolutions of 9Cr heat resistant steel deposited metals with different Si contents during 550°C aging process, J. Mater. Res. Technol. 26 (2023) 2122–2139.
21. L. Yang, F. Zhao, W. Ding, Laves phase evolution in China low-activation martensitic (CLAM) steel during long-term aging at 550°C, Mater. 13 (1) (2019) 154.
22. S. Chen, X. Jin, L. Rong, Microstructural Evolution and Mechanical Properties of Ultrafine-Grained Ferritic-Martensitic Steel During Thermal Aging, Metall. Mater. Trans. A 51 (2020) 5154–5168.
23. Y. Zhang, H. He, H. Wang, G. Chen, X. An, Y. Wang, Evolution of microstructure and mechanical properties of 9Cr ferrite/martensite steels with different Si content after long-term aging at 550°C, J. Alloys Compd. 873 (2021) 159817.
24. G. Tian, B. Mao, Y. Xu, L. Fu, Z. Zhang, Y. Wang, A. Shan, Investigation on gradual degradation of mechanical property and microstructure in 9% Cr heat-resistant steels via interrupted creep test, J. Mater. Sci. 58 (10) (2023) 4637–4656.
25. C. Han, H. Xu, Y. Sun, T. Li, J. Huang, X. Che, L. Chen, Effect of Final Rolling Temperature on the Precipitates and Strengthening-Toughening Mechanism of V-N Microalloyed X70 Pipeline Steel, Steel Res. Int. (2025) 2500562.
26. A. Fedoseeva, V. Dudko, N. Dudova, R. Kaibyshev, Effect of Co on the strengthening mechanisms of the creep-resistant 9% Cr-2% W-MoVNb steel, J. Mater. Sci. 57 (46) (2022) 21491–21501.
27. Q. Li, Modeling the microstructure–mechanical property relationship for a 12Cr-2W-V-Mo-Ni power plant steel, Mater. Sci. Eng. A 361 (1–2) (2003) 385–391.
28. J. Ren, L. Yu, Y. Liu, C. Liu, H. Li, J. Wu, Effects of Zr addition on strengthening mechanisms of Al-alloyed high-Cr ODS steels, Materials 11 (1) (2018) 118.
29. E.G. Astafurova, G.G. Maier, S.V. Astafurov, Effect of Vanadium-Alloying on Microstructural Evolution and Strengthening Mechanisms of High-Nitrogen Steel Processed by High-Pressure Torsion, Phys. Mesomech. 27 (6) (2024) 747–759.